NANO LETTERS

2007
Vol. 7, No. 1
51−57

Factors Controlling the Electrodeposition of Metal Nanoparticles on Pristine Single Walled Carbon Nanotubes

Thomas M. Day, Patrick R. Unwin, and Julie V. Macpherson*

Department of Chemistry, University of Warwick, Coventry CV4 7AL, United Kingdom

Received August 22, 2006; Revised Manuscript Received November 8, 2006

ABSTRACT

The electrodeposition of metal (Pd and Pt) nanoparticles on networks of pristine single walled carbon nanotubes (SWNTs) has been investigated using a microelectrochemical cell. A microcapillary containing electrolyte solution and a reference electrode is contacted with a silicon oxide substrate bearing a SWNT network, connected as the working electrode. Electrodeposition is promoted by applying a potential between the SWNT network and the reference electrode. By combination of analysis of the resulting current–time curves with atomic force microscopy and field emission scanning electron microscopy imaging of the network surfaces after electrodeposition, the nature of metal nanoparticle formation on SWNTs has been elucidated. In particular, the parameters controlling nanoparticle number density, distribution, and size have been identified, with short deposition times and high driving forces favoring the formation of ultrasmall particles at high density. Capacitance and network resistance effects are minimized in the microcapillary configuration, making it possible to accurately analyze short time-scale deposition processes (millisecond time scale). Furthermore, it is also possible to make many measurements on a pristine sample, simply by moving the position of the microcapillary to a new location on the substrate.

Metal nanoparticles and nanowires are proving to be a significant class of materials for a wide variety of applications. For example, immobilized Pd and Pt nanoparticles have potential use in fuel cell electrodes[1] and in catalysis,[2] while nanowires have been utilized for sensing applications.[3] Important considerations in the manufacture of these materials are control over the physical dimensions and, for immobilized materials, location on the substrate of interest. As the characteristic properties of nanomaterials may depend critically on size,[4] it is desirable that experimental parameters can be tuned to allow optimized nanostructure formation. In this context, electrochemical techniques are particularly attractive for the electrodeposition of metallic nanostructures,[5] since parameters such as deposition potential, time, and solution composition can be varied, so as to control growth rate, particle size, and number density.

The substrate onto which metal nanostructures are deposited may have a significant influence on the morphology of the resulting structure, with the substrate in some cases acting as a template. The use of single walled carbon nanotubes (SWNTs) for the deposition of metallic structures is of considerable interest,[6] and the electrolytic formation of such structures has recently been demonstrated.[7−10] Metal nanoparticles have been electrodeposited onto two-dimensional SWNT networks,[7,8] and the growth of a single Pt nanoparticle at the end of a SWNT has been described. Voltammetric studies[7−9] have also demonstrated that metal nanoparticles formed in this way are electrically wired to the SWNTs.

Nanoparticles are characterized by ultrahigh mass transport rates, provided they are spaced sufficiently far apart to prevent overlap of diffusion fields from neighboring particles. Wired nanoparticles in this arrangement would be attractive for nanoscale electrochemical studies.[11] On the other hand, nanowire formation requires that nanoparticles are arranged contiguously. Thus, in order to create a nanostructured interface of interest, it is clear that the kinetics of nanoparticle formation is understood, so that nanoparticle size and density can be controlled.

In this Letter we investigate the electrodeposition of metal nanoparticles on SWNT networks, using a microcapillary electrochemical cell. A microcapillary (orifice opening in the range 20−80 μm for the studies described herein) filled with the metal salt solution of interest and a reference electrode is placed in contact with a pristine SWNT network, which is connected as a working electrode. With the ability to position the capillary at many different locations on the network, it is possible to systematically investigate the effect of electrode potential and deposition time on the nanoparticle formation process. Moreover, the sample surface is guaranteed to be free from photoresist processing which others have

* Corresponding author: j.macpherson@warwick.ac.uk; +44(0)2476 573886.

10.1021/nl061974d CCC: $37.00
Published on Web 12/15/2006

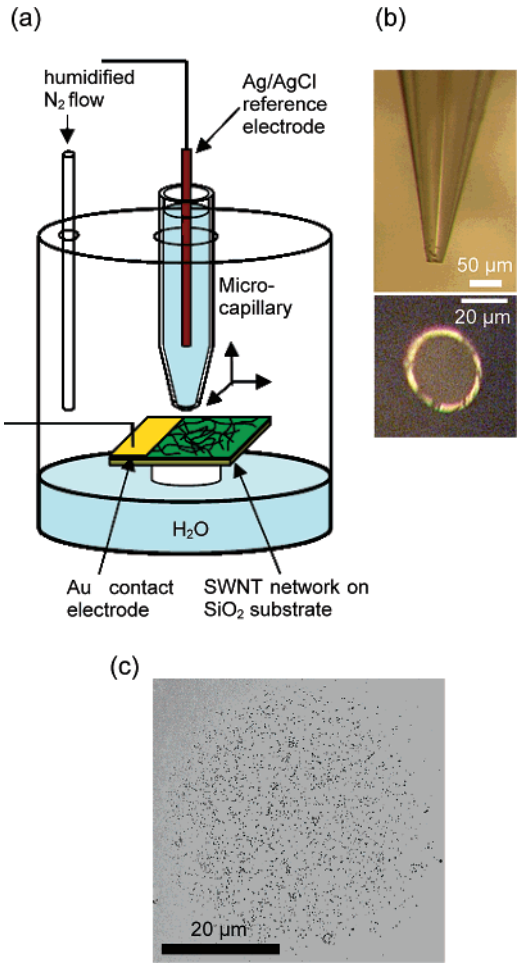

Figure 1. (a) Schematic of the microcapillary experimental setup. The substrate comprised a two-dimensional interconnected network of SWNTs on a Si/SiO_2 surface. A gold band was evaporated onto the substrate to electrically connect the SWNTs. A microcapillary, containing the electrodeposition solution, was positioned at different locations on the substrate using *x*,*y*,*z* micropositioners. The "moat" of water and humidified N_2 kept the humidity of the cell high, preventing solution evaporation from the microcapillary. (b) Optical images of the tip of a typical microcapillary side-on (top image) and end-on (bottom image). (c) FE-SEM image showing an area of electrolytically deposited Pt nanoparticles (deposition time and potential of 30 s and −0.3 V, respectively) on a SWNT network over an area defined by the inner dimensions of the microcapillary.

suggested may contaminate SWNTs if not removed successfully.[12] Finally, this approach offers the possibility for selectively patterning metal nanoparticles in defined areas of a SWNT network.

Microcapillary electrochemical cells have mainly found application in the investigation of localized corrosion processes,[13] while nanopipets, under potential control, have been used to deposit biomolecules in defined locations on surfaces.[14] An attractive feature of the microcapillary method is that small regions of a substrate surface can be electrochemically characterized or modified independently of the rest of the substrate. Moreover, network resistive and capacitative effects are minimized, allowing the measurement of faradaic processes on short time scales.

Figure 1a illustrates the experimental setup employed in our studies. A borosilicate capillary (1.2 mm outer diameter, 0.69 mm internal diameter, Harvard Apparatus Ltd.), pulled to a defined small opening using a laser pipet puller (model P-2000, Sutter Instrument Co.), was polished flat (0.1 μm polishing pad, Buehler), as shown in the optical image in Figure 1b. The capillary, filled with electrolyte solution and housing a Ag/AgCl wire electrode of stable potential,[15] was connected to a three-axis (*x*, *y*, *z* arrangement) micromanipulator (Newport Corp.). The capillary was lowered toward the surface of interest, using the *z*-micropositioner until it just made contact with the substrate (procedure observed using a video microscope (Baxall Ltd., U.K.)). The substrate was connected electrically as a working electrode using wire bonded to an evaporated gold band deposited over part of the SWNT network. After an electrochemical measurement had been made, the capillary was moved to new locations for subsequent measurements.

The SWNTs were grown directly onto a 5 mm^2 Si/SiO_2 surface by catalyzed chemical vapor deposition (cCVD), forming a two-dimensional network.[7,16] The substrates used in this study had SWNT densities in the range 8−15 μm length of SWNT per μm^2 of substrate, i.e., well above the percolation threshold for metallic SWNTs (mSWNTs).[17] Of importance was the ability to create a known, reproducible contact between the solution in the capillary and the surface, ideally defined by the inner diameter of the capillary. Previous applications of microcapillaries in corrosion studies used a silicone gasket seal at the end of the capillary. However, to avoid any possibility of surface contamination, clean silicone-free capillaries were employed. To eliminate evaporation effects, a humidity cell was constructed (see schematic in Figure 1a), where the surrounding atmosphere was saturated with H_2O.

Trial cyclic voltammetry (CV) experiments, with the humidity cell, were made with a microcapillary filled with a solution containing 1 mM $Ru(NH_3)_6^{3+}$ (with 1 M KNO_3 as supporting electrolyte) in contact with a gold working electrode surface (see Supporting Information). From the CVs recorded at scan rates in the range 0.01−2 V s^{-1}, the relationship between the measured peak current and scan rate was as expected, based on linear diffusion to the electrode surface with an area defined by the inner dimensions of the capillary (77 μm). Note that the cone angle of the capillary is such that the assumption of linear diffusion is appropriate. These results indicate that when a solution-filled microcapillary is positioned in contact with a substrate surface, an area of the surface corresponding to the opening of the microcapillary is typically exposed to the electrolyte solution. Moreover, this area was found to remain constant over the time scale of a set of voltammetric measurements. As the high-density SWNT network surface is more hydrophobic than the Au surface, one would also expect the ready confinement of solution to an area defined by the microcapillary in the SWNT network experiments. Evidence that this is the case is provided by Figure 1c, which shows an area in which Pt nanoparticles were deposited in a typical experiment. The capillary used had an inner diameter of 35 μm, which correlates well with the area defined by the metal deposition pattern.

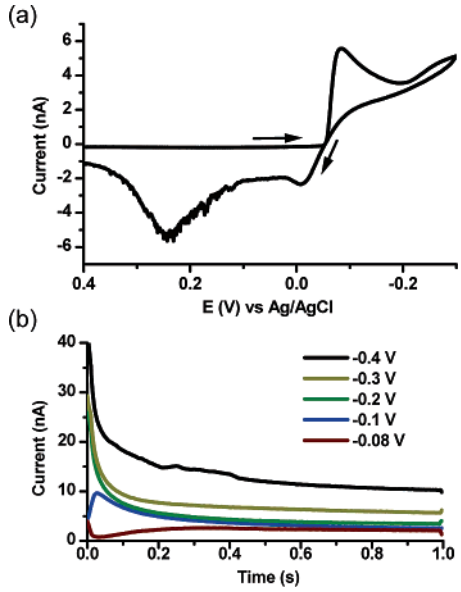

Figure 2. (a) Cyclic voltammogram for the deposition and stripping of Pd on a SWNT network using a microcapillary cell (solution contained 1 mM $Pd(NO_3)_2$, 3.6 mM HNO_3 and 1 M KNO_3) at a scan rate of 0.05 V s^{-1}. (b) Current−time transients for the deposition of Pd onto a SWNT network electrode for 1 s at deposition potentials between −0.08 and −0.4 V (vs Ag/AgCl) from open circuit. Microcapillary was 65 μm i.d.

Figure 2a shows a typical CV (scan rate 0.05 V s^{-1}) for the localized deposition of Pd on a SWNT network (area defined by microcapillary 65 μm i.d.) from a solution containing 1 mM $Pd(NO_3)_2$ in 3.6 mM HNO_3 and 1 M KNO_3. When the substrate potential is scanned cathodically, a current peak for the reduction of Pd^{2+} to Pd is observed at ca. −0.06 V versus Ag/AgCl, while Pd stripping is noted upon reversing the scan direction (ca. 0.25 V). This behavior is consistent with that observed by Penner et al. for the deposition and removal of Pd on a highly ordered pyrolytic graphite electrode.[18] The rising current at potentials more negative than −0.2 V is due to proton reduction to hydrogen. The reoxidation of hydrogen is seen on reversing the scan direction, at ca. 0.0 V.

To determine the effect of various parameters on metal electrodeposition, current−time ($i-t$) transients were recorded in which the substrate electrode potential was stepped from open circuit to a series of potentials beyond the diffusion-limited peak at −0.08 V, indicated in Figure 2a. These results and the others presented in this Letter are representative of many measurements made (>10) for each parameter investigated. Repeat measurements were possible on the same sample, due to the ease with which the capillary could be moved to a new location on the surface. An example family of $i-t$ curves is shown in Figure 2b, obtained with a microcapillary positioned approximately 40 μm from the Au contact at a series of fresh locations parallel to the contact band. At the lowest driving potential (−0.08 V), after an initial charging current decay, the current can be seen to rise with time (over a period of ca. 0.3 s). This corresponds to the growth of Pd deposits which are initially sufficiently small and well separated that the individual diffusion fields do not overlap. The particles grow in size, and may increase in number, so that the active electrode area and current increases. This behavior is also evident in the data at −0.1 V, although it is compressed into the first 0.025 s. After this, the current reaches a maximum and then decreases with time. This is due to the overlap of diffusion fields of neighboring particles, so that a predominantly linear diffusion field is established, resulting in the observed current−time characteristic. As the deposition potential becomes more cathodic, the transition from individual to collective behavior occurs on a shorter time scale, so that the $i-t$ characteristics approach a Cottrellian response,[19] as can be seen in Figure 2b, for the case of −0.2 V. The current response at more cathodic potentials (−0.3 and −0.4 V) follows the same trend, but the current is higher than expected at long times due to a contribution to the current from the reduction of protons, evident in the CV data in Figure 2a.

To obtain further insights into the electrodeposition process, atomic force microscopy (AFM, Veeco Multimode AFM with Nanoscope IIIa controller) and field emission-scanning electron microscopy (FE-SEM, Zeiss SUPRA 55 VP) were employed to characterize the morphology of the metal structures. Figure 3a shows a series of representative FE-SEM images of Pd nanoparticles electrodeposited onto a SWNT network at potentials in the range (i) −0.1 V, (ii) −0.15 V, (iii) −0.2 V, (iv) −0.25V, (v) −0.3 V, (vi) −0.35 V, and (vii) −0.4 V vs a Ag/AgCl reference electrode, for a period of 1 s. The $i-t$ data for (i), (iii), (v), and (vii) are shown in Figure 2b.

Each image is 2 μm by 2 μm and is representative of Pd deposition. At most of the potentials there appears to be preferential deposition of Pd on particular SWNTs, while for significant areas of the surface there is no deposition, particularly at the lower driving potentials. This pattern of nanoparticle deposition can be seen over longer length scales, as shown in Figure 4, which illustrates deposition at −0.2 V and −0.4 V (1 s deposition time). These data are taken from the same set of experiments as presented in Figures 2 and 3.

The preferential deposition at low driving force could be due to the presence of both metallic and semiconducting SWNTs in the network, in an approximately 1:2 ratio.[20] Deposition might be expected to take place preferentially on the metallic SWNTs, although the electroactivity of the semiconducting SWNTs will be sensitive to the solution conditions and applied potential.[21,22] Other factors may also come into play; for example, it has been shown theoretically that the diameter and chirality of SWNTs may affect the electron-transfer kinetics, which would be expected to impact on metal nucleation rates.[23] It has also been demonstrated experimentally that at *very low* deposition overpotentials (10−50 mV), nucleation takes place preferentially at defect sites on the SWNTs, although, it was not possible to distinguish the chemical nature of the defect sites.[10] Clearly, the defect density in SWNTs will depend on the growth procedure, but in previous studies of cCVD grown SWNTs, defect spacings of 0.36 μm (s.d. = 0.33 μm) were reported.[10] This is consistent with defect density spacings measured on our SWNTs using electrically based scanned probe micros-

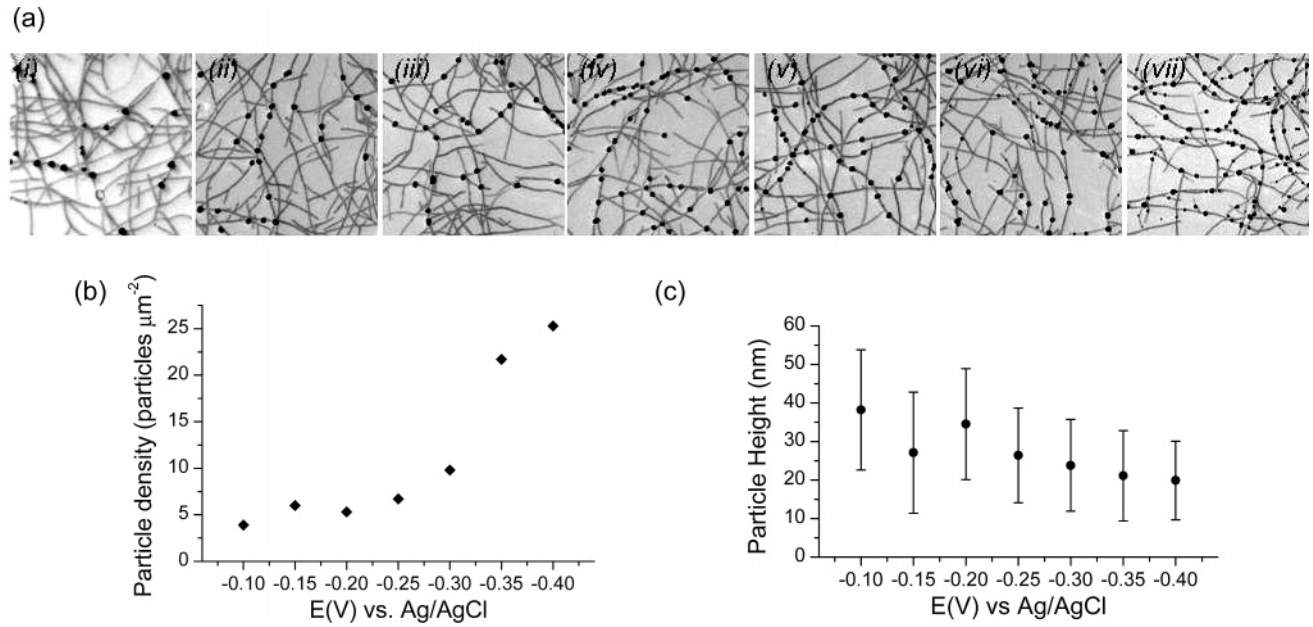

Figure 3. (a) FE-SEM images (2 μm × 2 μm) of Pd nanoparticles deposited on a SWNT network at (i) −0.1 V, (ii) −0.15 V, (iii) −0.2 V, (iv) −0.25 V, (v) −0.3 V, (vi) −0.35 V, and (vii) −0.4 V, for 1 s. (b) Plot of particle density vs deposition potential. (c) Plot of mean particle height (taken from AFM analysis) vs deposition potential. The error bars correspond to one standard deviation from the mean height. Capillary was 65 μm i.d.

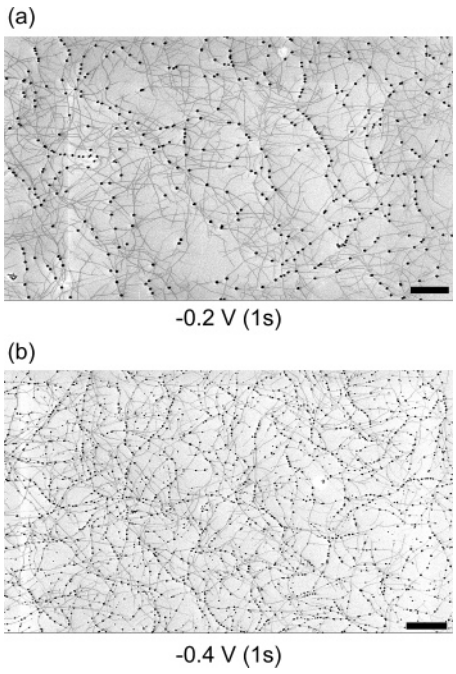

Figure 4. FE-SEM images of Pd deposition onto SWNTs at (a) −0.2 V and (b) −0.4 V for 1 s. Scale bars represent 1 μm.

copy techniques.[24] The results presented in this paper clearly demonstrate that with increasing driving force, nanoparticles form with a greatly increased surface density, suggesting that growth takes place on nondefected regions of the SWNT as we and others (referred to as random nucleation) found previously.[10]

Figure 3b summarizes the variation of particle number density with applied deposition potential, derived from the data in Figure 3a. There is a significant trend of increase in nanoparticle number density with increasing driving potential. AFM was used to quantify particle size at the different driving potentials, in terms of particle height rather than width to avoid tip convolution effects; the results are summarized in Figure 3c. Although there is some variance in particle height at each potential, the height can be seen to generally decrease with increasing deposition potential. This trend can be rationalized because the increased density of nanoparticles formed results in a diminution in the flux to each particle (in a linear diffusion regime). Integration of the $i-t$ curves in Figure 2b provides the total charge passed, and with knowledge of the particle number density (Figure 3b) the expected nanoparticle size can be determined. Assuming a spherical shape for the particles, the radius of each particle is given by eq 1[25]

$$r = \left(\frac{3QM}{4\pi nF\rho}\right)^{1/3} \quad (1)$$

where Q is the charge passed per particle, M and ρ are the molar mass and density of the deposited species (106.42 g mol^{-1} and 12.023 g cm^{-3} for Pd), n (=2) is the number of electrons transferred, and F = 96485 C mol^{-1}. These simple calculations, which assume that the number of particles is time-invariant (vide infra), also predict a slight decrease in mean particle size, as shown in Table 1.

Figure 5 summarizes the effect of deposition time on the electrodeposition of Pd on SWNT networks for a deposition potential of −0.1 V, with times in the range 0.001−10 s. Typical FE-SEM images of electrodeposition are shown in Figure 5a. The electrodeposition potential was set at a value where deposition was diffusion-limited (−0.1 V versus Ag/AgCl), but where the current response was not complicated by proton reduction. A capillary of 41 μm i.d. was employed for these measurements.

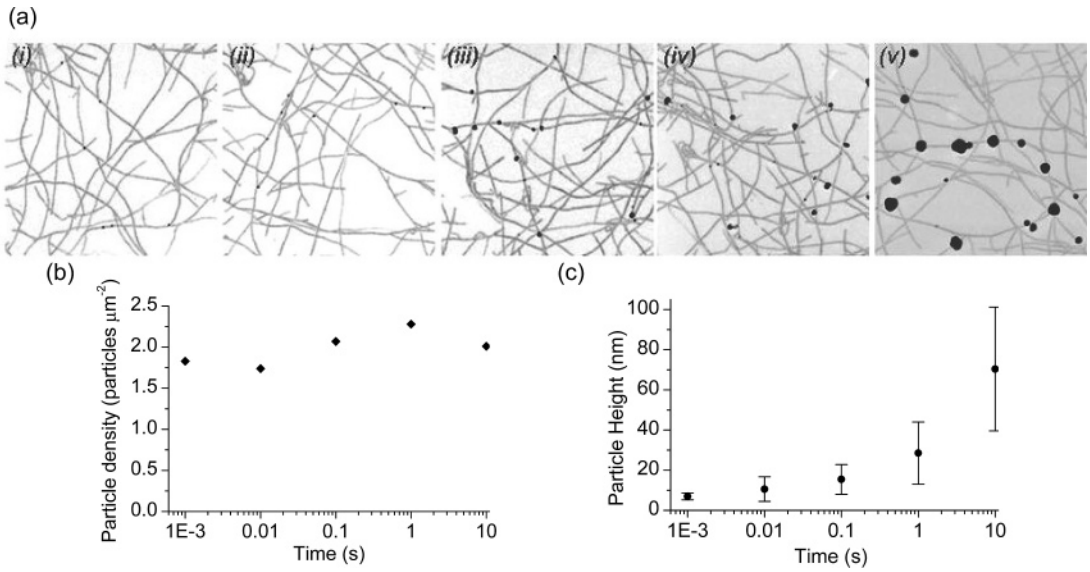

Figure 5. (a) FE-SEM images (2 μm × 2 μm) of Pd nanoparticles deposited onto a SWNT network at −0.1 V for (i) 0.001 s, (ii) 0.01 s, (iii) 0.1 s, (*iv*) 1 s, and (v) 10 s. (b) Plot of mean Pd particle density against time for the above depositions. (c) Plot of Pd particle heights (taken from AFM analysis) for the above depositions. The bars correspond to 1 standard deviation from the mean particle height. Capillary was 41 μm i.d.

Table 1. Measured Nanoparticle Heights from the Data in Figure 3, Compared to Calculated Values (Eq 1) Assuming Spherical Nanoparticles

potential (V) vs Ag/AgCl	mean particle height (nm) ±1 s.d. (exptl)	spherical particle height (nm) (calcd from eq 1)
−0.10	38.2 ± 15.6	30.1
−0.15	27.1 ± 15.7	28.3
−0.20	34.5 ± 14.4	28.5
−0.25	26.4 ± 12.3	29.6
−0.30	23.8 ± 11.9	27.2
−0.35	21.1 ± 11.7	23.5
−0.40	19.9 ± 10.2	24.3

The five measurements demonstrate that the particle density remains approximately constant (Figure 5b) over a long time period (0.001−10 s), with deposition occurring with an approximately constant density of particles, resulting in an increase in particle size (expressed as a height) with deposition time (Figure 5c). The essentially time-invariant particle density indicates that the nucleation of particles occurs on a very rapid time scale (submilliseconds). It is also clear that by using very short deposition times, one can form ultrasmall monodisperse particles (7.0 ± 1.7 nm; Figure 5a(i)).

There have been many attempts to model diffusion-controlled growth in order to extract nucleation parameters, such as nucleation numbers, from experimental $i-t$ transients. The most widely used methods are based on Avrami's theorem[26] and an original model developed by Scharifker and Hills[27] (the SH model) from which most other models have stemmed.[28] The SH model gives expressions for the current density I_t at time, t, for the limiting cases of instantaneous and progressive nucleation. Although the operation of a truly instantaneous mechanism has been disputed,[29] the fact that the density of nanoparticles formed remains constant down to times as short as milliseconds makes this a useful model to which the data can be compared. The instantaneous SH model predicts that $i-t$ transients are of the following form

$$I_t = \frac{zFD^{(1/2)}c}{\pi^{(1/2)}t^{(1/2)}}[1 - \exp(-N_0\pi kDt)] \qquad (2)$$

where z is the number of electrons transferred, D is the diffusion coefficient of the species of interest, c is the bulk concentration of this species, N_0 is the nucleation site density (assumes randomly spaced sites), and

$$k = \left(\frac{8\pi cM}{\rho}\right)^{1/2} \qquad (3)$$

D for Pd^{2+} was determined to be 7.2×10^{-6} cm^2 s^{-1} via the steady-state diffusion-limited current recorded at a 12.5 μm radius mercury hemisphere electrode, placed in the palladium plating solution.

Figure 6a shows a series of $i-t$ transients for the electrodeposition of Pd on SWNTs at potentials between −0.06 and −0.14 V for 1 s. The transients at −0.08, −0.10, and −0.14 V all show a current peak, which increases in magnitude and occurs at shorter times with increasing driving potential. At longer times the currents decrease and coincide, demonstrating that the electrode areas are equivalent and that planar diffusion is established. As highlighted above, the occurrence of a current peak is indicative of a transition time. The $i-t$ curve for −0.06 V deposition shows no peak, and the current simply increases with time, suggesting that even after 1 s there is insufficient overlap between diffusion fields for the deposition to become diffusion-controlled. Referring to the CV in Figure 2a, it can be seen that at −0.06 V the deposition process is only just established.

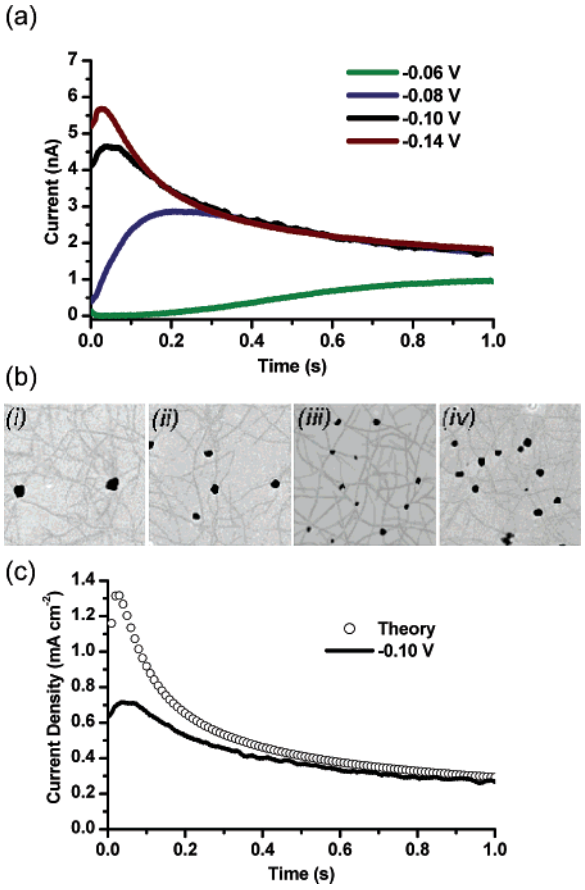

Figure 6. (a) Current−time transients for the electrodeposition of Pd onto a SWNT network at −0.06 (bottom curve), −0.08, −0.10, and −0.14 V (top curve) versus Ag/AgCl for 1 s (capillary 30 μm i.d.). (b) FE-SEM images (2 μm × 2 μm) of Pd nanoparticles deposited from the transients shown in (a): (i) −0.06 V, (ii) −0.08 V, (iii) −0.10 V, and (iv) −0.14 V. (c) Current density−time transient at −0.1 V from (a), compared with a theoretical transient calculated using eq 2 ($D = 7.2 \times 10^{-6}$ cm^2 s^{-1} and $N_0 = 1.5 \times 10^8$ cm^{-2}).

Figure 6c shows the transient for −0.10 V, expressed as current density, compared to eq 2. There are no adjustable parameters, and the value for N_0, determined from FE-SEM images, was 1.5×10^8 cm^{-2}. The theory and experimental transients tend to similar values toward long times of 1 s, consistent with a Cottrellian response. However, at shorter times, the experimental peak current is much lower than expected based on eq 2. This may be due to a kinetic limitation at short times,[30] but also the nonuniformity of the surface could play a role (SWNTs cover less than a 1% of the surface), especially if deposition involves surface diffusion of ad-atoms. Certainly, the nonuniform distribution of growth centers will significantly influence the $i-t$ transient behavior at short to medium times, as the particle distributions shown in this paper indicate that there will be overlap of diffusion fields of neighboring particles on an SWNT at very short times and then overlap of diffusion fields of adjacent active tubes on a longer time scale.

While the main focus of this work has been on Pd deposition, the formation of supported Pt nanoparticles is also of considerable interest, especially in the form of a Pt−carbon composite.[31] Figure 7a shows a series of $i-t$ curves

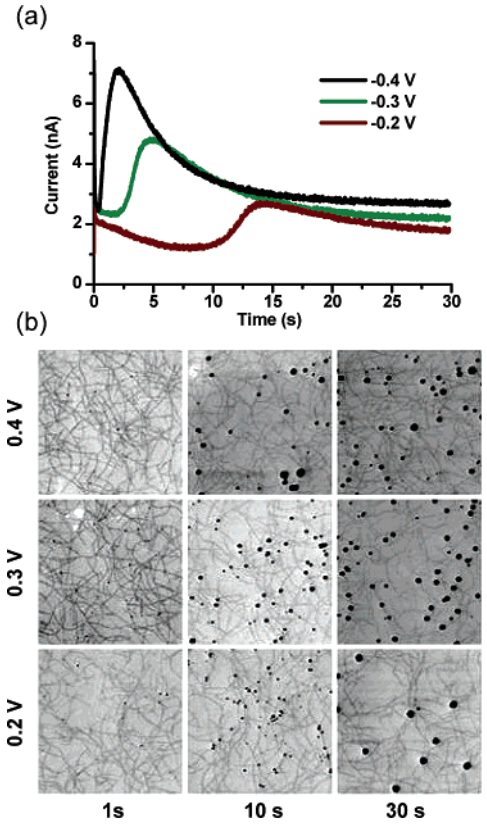

Figure 7. (a) Current−time transients for the deposition of Pt onto SWNTs for 30 s at −0.2, −0.3, and −0.4 V (vs Ag/AgCl). Solution contained 1 mM K_2PtCl_6 and 0.5 M $HClO_4$. (b) FE-SEM images (5 μm × 5 μm) of Pt on SWNTs at −0.2, −0.3, and −0.4 V for 1, 10, and 30 s.

for Pt deposition at different driving potentials over a period of 30 s. The potential at which Pt electrodeposition starts is ca. −0.1 V (as determined from CVs recorded in the Pt plating solution, in a similar way as in Figure 2a), compared with −0.06 V for Pd. Therefore, the electrode potentials used for Pt electrodeposition (−0.2, −0.3, and −0.4 V) cover a similar range of driving forces as for Pd deposition. Figure 7b shows FE-SEM images recorded at times of 1, 10, and 30 s at different driving potentials.

The $i-t$ curves in Figure 7a contrast markedly with those in Figures 2b and 5a for Pd. In particular, the nucleation and growth process appears to be much slower for Pt, as evidenced by the longer times at which the current peak occurs. This is not unexpected given that Pt deposition from $PtCl_6^{2-}$ is a complex multistep process.[32] Moreover, the FE-SEM data indicate that the nanoparticle number density is not constant with time, clearly pointing toward a progressive nucleation mechanism.

In conclusion, using a microcapillary technique we have shown how key features in the electrodeposition of metal nanoparticles on SWNT networks can be determined. In particular, as shown in detail for Pd, control over the deposition potential and time allows the number density, distribution, and nanoparticle size to be controlled. The microcapillary technique also enables multiple measurements to be made on the same SWNT network substrate, without the need for lengthy lithographic procedures, so that SWNTs

are studied under truly pristine conditions. The technique can be compared to scanning electrochemical microscopy (SECM), which has also been used to locally deposit metallic structures on surfaces.[33] However, the microcapillary technique offers several advantages over SECM, including: greater versatility, with the possibility of depositing a wider range of materials; only a small fraction of the surface is in contact with solution for a short period of time minimizing extraneous deposition. Moreover in SECM the tip electrode−substrate separation needs to be known and this can sometimes be difficult to determine (e.g., the need for another electroactive mediator in solution).

Acknowledgment. We thank Steve York for help with FE-SEM and Dr. Neil Wilson (Department of Physics, University of Warwick) for helpful suggestions. J.V.M. thanks the Royal Society for a Research Fellowship and EPSRC for support (GR/S24138/01 and EP/C518268/1).

Supporting Information Available: Details of cyclic voltammetry experiments and analysis to validate the use of the microcapillary cell for the analysis of redox processes on conducting surfaces. This material is available free of charge via the Internet at http://pubs.acs.org.

References

(1) (a) Joo, S. H.; Choi, S. J.; Oh, I.; Kwak, J.; Liu, Z.; Terasaki, O.; Ryoo, R. *Nature* **2001**, *412*, 169. (b) Steigerwalt, E. S.; Deluga, G. A.; Cliffel, D. E.; Lukehart, C. M. *J. Phys. Chem. B* **2001**, *105*, 8097. (c) Parsons, R.; VanderNoot, T. *J. Electroanal. Chem.* **1988**, *257*, 9.
(2) (a) Bell, A. T. *Science* **2003**, *299*, 1688. (b) Niu, Y. H.; Yeung, L. K; Crooks, R. M. *J. Am. Chem. Soc.* **2001**, *123*, 6840. (c) Reetz, M. T.; Westermann, E. *Angew. Chem., Int. Ed.* **2000**, *39*, 165.
(3) (a) Cui, Y.; Wei, Q.; Park, H.; Lieber, C. M. *Science* **2001**, *293*, 1289. (b) Murray, B. J.; Walter, E. C.; Penner, R. M. *Nano Lett.* **2004**, *4*, 665. (c) Im, Y.; Lee, C.; Vasquez, R. P.; Bangar, M. A.; Myung, N. V.; Menke, E. J.; Penner, R. M.; Yun, M. *Small* **2006**, *2*, 356.
(4) (a) Zoval, J. V.; Stiger, R. M.; Biernacki, R. R.; Penner, R. M. *J. Phys. Chem.* **1996**, *100*, 837. (b) Schmid, G. *Chem. Rev.* **1992**, *92*, 1709.
(5) Penner, R. M. *J. Phys. Chem. B* **2002**, *106*, 3339 and references therein.
(6) (a) Tinkham, M.; Lau, C. N.; Bezryadin *Nature* **2000**, *404*, 971. (b) Kong, J.; Chapline, M. G.; Dai, H. *Adv. Mater.* **2001**, *13*, 1384.
(7) Day, T. M.; Unwin, P. R.; Wilson, N. R.; Macpherson, J. V. *J. Am. Chem. Soc.* **2005**, *127*, 10639.
(8) Quinn, B. M.; Dekker: C.; Lemay, S. G. *J. Am. Chem. Soc.* **2005**, *127*, 6146.
(9) Quinn, B. M.; Lemay, S. G. *Adv. Mater.* **2006**, *18*, 855.
(10) Fan, Y.; Goldsmith, B. R.; Collins, P. G. *Nat. Mater.* **2005**, *4*, 906.
(11) Slevin, C. J.; Gray, N. J.; Macpherson, J. V.; Webb, M. A.; Unwin, P. R. *Electrochem. Commun.* **1999**, *1*, 282.
(12) Heller, I.; Kong, J.; Heering, H. A.; Williams, K. A.; Lemay, S. G.; Dekker, C. *Nano Lett.* **2005**, *5*, 137.
(13) (a) Suter, T.; Böhni, H. *Electrochim. Acta* **1997**, *42*, 3275. (b) Suter, T.; Böhni, H. *Electrochim. Acta* **1998**, *43*, 2843. (c) Krawiec, H.; Vignal, V.; Oltra, R. *Electrochem. Commun.* **2004**, *6*, 655.
(14) (a) Bruckbauer, A.; Ying, L. M.; Rothery, A. M.; Zhou, D. J.; Shevchuk, A. I.; Abell, C.; Korchev, Y. E.; Klenerman, D. *J. Am. Chem. Soc.* **2002**, *124*, 8810. (b) Bruckbauer, A.; Zhou, D. J.; Ying, L. M.; Korchev, Y. E.; Abell, C.; Klenerman, D. *J. Am. Chem. Soc.* **2003**, *125*, 9834.
(15) Macpherson, J. V.; Unwin, P. R. *J. Phys. Chem.* **1995**, *99*, 14824.
(16) Hafner, J. H.; Cheung, C. L.; Oosterkamp, T. H.; Lieber, C. M. *J. Phys. Chem. B* **2001**, *105*, 743.
(17) Wilson, N. R.; Guille, M.; Dumitrescu, I.; Fernandez, V. R.; Rudd, N. C.; Williams, C. G.; Unwin, P. R.; Macpherson, J. V. *Anal. Chem.* **2006**, *78*, 7006.
(18) Favier, F.; Walter, E. C.; Zach, M. P.; Benter, T.; Penner, R. M. *Science* **2001**, *293*, 2227.
(19) Bard, A. J.; Faulkner, L. R. *Electrochemical Methods, Fundamentals and Applications*; John Wiley: New York, 2001; p 163.
(20) Saito, R.; Dresselhaus, G.; Dresselhaus, M. S. *Physical Properties of Carbon Nanotubes*; Imperial College Press: London, 1998.
(21) Day, T. M.; Wilson, N. R.; Macpherson, J. V. *J. Am. Chem. Soc.* **2004**, *126*, 10639.
(22) Rosenblatt, S.; Yaish, Y.; Park, J.; Gore, J.; Sazonova, V.; McEuan, P. L. *Nano Lett.* **2002**, *2*, 869.
(23) Heller, I.; Kong, J.; Williams, K. A.; Deeker, C.; Lemay, S. G. *J. Am. Chem. Soc.* **2006**, *128*, 7353.
(24) Wilson, N. R. Unpublished results and paper in preparation.
(25) Guo, J.; Tokimoto, T.; Othman, R.; Unwin, P. R. *Electrochem. Commun.* **2003**, *5*, 1005.
(26) (a) Avrami, M. *J. Chem. Phys.* **1939**, *7*, 1103. (b) Avrami, M. *J. Chem. Phys.* **1940**, *8*, 212. (c) Avrami, M. *J. Chem. Phys.* **1941**, *9*, 177.
(27) Scharifker, B. R.; Hills, G. J. *Electrochim. Acta* **1983**, *28*, 879.
(28) (a) Sluyters-Rehbach, M.; Wijenberg, J. H. O. J.; Bosco, E.; Sluyters, J. H. *J. Electroanal. Chem.* **1987**, *236*, 1. (b) Mirkin, M. V.; Nilov, A. P. *J. Electroanal. Chem.* **1990**, *283*, 35. (c) Heerman, L.; Tarallo, A. *J. Electroanal. Chem.* **1999**, *470*, 70.
(29) (a) Deutscher, R. L.; Fletcher, S. *J. Electroanal. Chem.* **1988**, *239*, 17. (b) Deutscher, R. L.; Fletcher, S. *J. Electroanal. Chem.* **1990**, *277*, 1.
(30) Fletcher, S. *J. Cryst. Growth* **1983**, *63*, 505.
(31) (a) Gloaguen, F.; Léger, J.-M.; Lamy, C. *J. Appl. Electrochem.* **1997**, *27*, 1052. (b) Park, S.; Xie, Y.; Weaver, M. J. *Langmuir* **2002**, *18*, 5792. (c) Li, W.; Liang, C.; Zhou, W.; Qiu, J.; Zhou, Z.; Sun, G.; Xin, Q. *J. Phys. Chem. B* **2003**, *107*, 6292.
(32) Georgolios, N.; Jannakoudakis, D.; Karabinas, P. *J. Electroanal. Chem.* **1989**, *264*, 235.
(33) Scanning Electrochemical Microscopy; Bard, A. J., Mirkin, M. V., Eds.; Marcel Dekker: New York, 2001; Chapter 13.

NL061974D